Available online at www.eccomasproceedia.org
Eccomas Proceedia COMPDYN (2021) 546-562

ECCOMAS
Proceedia

COMPDYN 2021
8th ECCOMAS Thematic Conference on
Computational Methods in Structural Dynamics and Earthquake Engineering
M. Papadrakakis, M. Fragiadakis (eds.)
Streamed from Athens, Greece, 28 - 30 June 2021

LATTICE DISCRETE MODELING OF OUT-OF-PLANE BEHAVIOR OF IRREGULAR MASONRY

Micaela Mercuri[1], Madura Pathirage[2], Amedeo Gregori[1] and Gianluca Cusatis[2]

[1]University of L'Aquila
Department of Civil, Building and Environmental Engineering, L'Aquila, Italy
e-mails: micaela.mercuri@graduate.univaq.it, amedeo.gregori@ing.univaq.it

[2] Northwestern University
Department of Civil and Environmental Engineering, Evanston, IL, USA
e-mails: madura.pathirage@u.northwestern.edu, g-cusatis@northwestern.edu

Abstract. *Stone masonry buildings are known to be highly vulnerable to seismic actions. In this context, the analysis of the out-of-plane response of unreinforced masonry structures is crucial. For this purpose, the Lattice Discrete Particle Model (LDPM) was employed to simulate the mechanical behavior of stone masonries up to their failure. Unlike commonly used continuum-based methods or simplified analytical models, that are often limited in modeling correctly complex failure mechanisms, LDPM is able to capture accurately crack distributions and failure patterns. LDPM describes the masonry at the scale of stones and takes into account their interactions through tailored constitutive equations for tensile, compressive, shear, and frictional behaviors. First, LDPM was validated against experimental results on masonry panels subjected to out-of-plane loading. Next, the vertical bending mechanism was studied in the cases of one- and two-story walls with and without openings. Finally, more complex mechanisms were considered where the damage evolution and the fracture propagation were analyzed for a set of panels assumed to be placed within the continuity of a facade. The overall results presented in this paper show that LDPM can realistically predict the collapse mechanisms associated with out-of-plane loading for different structural configurations and geometries.*

Keywords: Out-of-Plane Behavior, Earthquake, Lattice Discrete Particle Model, Stone Irregular Masonry, Local Collapse Mechanisms, Global Collapse Mechanisms

ISSN:2623-3347
Peer-review under responsibility of the organizing committee of COMPDYN 2021.
doi:10.7712/120121.8508.19419

1 INTRODUCTION

Unreinforced masonry structures often constitute a large part of the cultural and architectural heritage of historical cities, and they are known to be highly vulnerable to earthquakes. Commonly, masonry structures are made of multiple load-bearing walls placed in orthogonal planes and with flexible floor diaphragms [1]. When an earthquake occurs, masonry structures dissipate kinetic energy both at the structural and at the material levels [2, 3]. At the structural scale, several factors affect the global response: the slenderness of the load-bearing walls [4, 5], the connections between the walls and the horizontal members, which allows for the box behavior [6, 7, 8, 9], and the presence of specific rigid floor diaphragms [10, 11, 12, 13, 14, 15, 16]. At the material scale, the mechanical properties of the masonry constituents (mortar and stones) [17, 18, 19, 20] and the quality of the construction work [21, 22] greatly affect the overall response. During a seismic event, masonry walls are typically subjected to in-plane and out-of-plane motions. Whereas in-plane behavior is the topic of a large number of studies available in the literature, the out-of-plane behavior is often neglected. This paper focuses on the latter behavior, as one of the most common damage reported in post-seismic surveys is the failure of peripheral masonry walls. Indeed, the earthquake intensity required to obtain out-of-plane collapse of walls is lower than the one required for in-plane collapse [3].

Several analytical methods exist to analyze the out-of-plane behavior of masonry walls, namely force-equilibrium and displacement-based methods. The first type of formulation is based on the static equilibrium analysis of rigid body mechanisms and limit theorem of plasticity [23, 24, 25, 26, 27, 28, 29, 30, 31, 32]. Force-equilibrium methods are generally adopted for large scale analysis and are known to lead to rather conservative limit states [8]. On the other hand, displacement-based methods [33, 34, 35, 36, 37, 38, 39, 40, 41, 42, 43, 44] appear to better estimate the limit values of masonry walls in out-of-plane loading. The rigid-block assumptions are often adopted within the postulates of limit theorem analysis (no-tensile strength, infinite compressive strength and absence of sliding between blocks) [23]. A capacity curve describing the horizontal multiplier α (limit equilibrium of the system) as a function of displacement d can then be obtained. When the displacement is zero, the value $\alpha(0) = \alpha_0$ represents the activation of the overturning. The loss of equilibrium is attained when $d = d_u$ where by definition $\alpha(d_u) = 0$. This curve can also be expressed in terms of spectral acceleration versus spectral displacement curve [45] or in terms of force-displacement curve. The rigid-block method within the displacement-based formulation is chosen in this paper for one part of the analysis of the out-of-plane behavior of masonry walls.

More advanced descriptions of the out-of-plane behavior of masonry walls and in general of the mechanical behavior of stone masonry require numerical models. Different methods are available and correspond to different levels of modeling resolution and computational costs [46, 47]. The finite element method is often used and allows micro-, meso-, or macro-modeling and the reader is referred to [48], [49], and [50], respectively. Although successful for regular masonry, the meshing complexity and the lack of accurate constitutive equations limit this method. Discrete element methods have also been employed [51, 52, 53, 54]. Multiple structures such as one or two-story buildings were modeled using 2D and 3D discrete element method [55], but limitations were found especially in capturing realistic out-of-plane responses. Moreover, these simulations were unable to correctly describe the fracture initiation and propagation. Indeed, in quasi-brittle materials such as masonry, understanding the development of the fracture process zone is crucial. An accurate model must also be able to capture the effect of stress parallel to cracks on the size of the fractured zone as shown recently in [56, 57], which

might be important in large masonry structures often under multiaxial state of stresses. To overcome these limitations, the Lattice Discrete Particle Model (LDPM) [58, 59] is here adopted for the numerical modeling. This model was originally conceived to simulate the behavior of concrete and other granular materials at the meso-scale level by modeling the interaction between coarse aggregate pieces. It was recently applied successfully for the modeling of stone masonry structures [60, 61]. LDPM is able to simulate accurately the fracturing behavior from crack trigger to localization, propagation, and to global failure, by taking into account the material heterogeneity. The interaction between stone aggregates embedded in the irregular matrix of lime or clay mortar is explicitly considered through dedicated constitutive equations, defined in a vectorial form to account for the correct state of stresses in the material.

In this study, the numerical model is first explained and validated against a set of experimental data relevant to masonry panels subjected to out-of-plane loading conditions. Next, the numerical model is used to assess its capability to simulate local collapse mechanisms, more specifically the bending mechanism. Finally, more complex mechanisms are analyzed with multiple structural configurations to simulate masonry walls within the continuity of the facade and to study the effect of transversal walls, floors and roofs on the overall behavior.

For a thorough investigation of the topic presented in this paper, the reader is referred to recent work of Mercuri and coworkers [61].

2 NUMERICAL MODEL AND VALIDATION

2.1 The Lattice Discrete Particle Model

The Lattice Discrete Particle Model (LDPM) was proposed by Cusatis and coworkers [58, 59] to simulate concrete at the coarse aggregate level. This model has a unique capability in capturing crack distribution and damage in granular quasi-brittle materials. It has been adopted to simulate the mechanical behavior of concrete [59, 62], mortar [63, 64], fiber reinforced concrete [65, 66], or to reproduce multi-physics phenomena such as hygro-thermo-chemical processes, alkali-silica reaction, and aging [63, 67, 68]. This lattice discrete model was also used to simulate the mechanical behavior of reinforced and unreinforced stone masonry [60, 61].

In the LDPM formulation, the masonry stones are simulated as spherical particles (see Fig. 1a and b). They are placed randomly from the largest to the smallest size in a given volume of material. The particle size distribution follows a Fuller sieve curve defined from a set of mix-design parameters: cement-mortar content c, water-to-mortar ratio w/c, maximum and minimum stone size d_a and d_0, respectively, and Fuller coefficient n_f. Fig. 1e shows on an example the particle placement inside a dog-bone specimen. The geometry of the interaction between stone-particles is described as follows. First, a Delaunay tetrahedralization is performed with the centers of the particles to generate a lattice system (see Fig. 1c). Next, a domain tessellation is performed to identify the possible failure locations between adjacent stone-particles (see Fig. 1d). These two steps result in the generation of a system of polyhedral cells enclosing the particles (see Fig. 1f). These irregular cells idealize real textures and shapes of typical masonry stones and their surrounding mortar layer. The surface of each polyhedral cell is composed of triangular facets (see Fig. 1g) where the LDPM constitutive equations, facet stresses and strains are formulated in a vectorial form. The constitutive equations take into account the softening behavior for pure tension and shear-tension and the plastic hardening behavior for pure compression and shear-compression. For the complete set of constitutive equations, as well as the compatibility and equilibrium equations, and the numerical implementation, the reader is referred to the work of Cusatis and coworkers [58], and the recent work of Mercuri and coworkers [61].

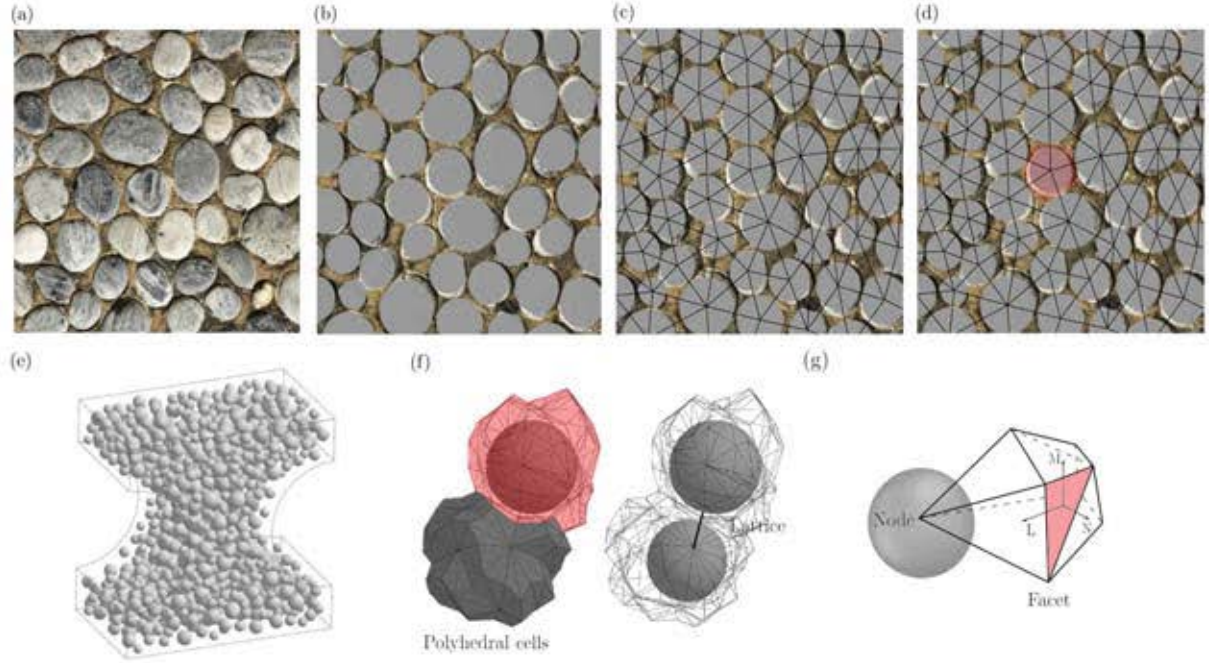

Figure 1: (a) 2D representation of irregular stone masonry; (b) approximation with spherical particles; (c) Delaunay tetrahedralization; (d) Domain tessellation and generation of a system of polyhedral cells; (e) particle distribution in a dogbone specimen; (f) two adjacent LDPM polyhedral cells enclosing two stones; (g) tetrahedron portion associated with a stone-particle and one triangular facet.

2.2 Validation with experimental data

2.2.1 Description of experiments and numerical modeling

The Lattice Discrete Particle Model is here validated against experimental data reported in Degli Abbati and coworkers [69]. The experiments consisted in loading in out-of-plane direction three masonry panels of different dimensions. The sizes of the specimens and their slenderness ratios are shown in Table 1. Lime mortar was used as binder in the preparation of the specimens. The stones were irregular with an average block size of $180 \times 120 \times 120$ mm. All the panels were built on top of a masonry base with a larger thickness. For the testing setup, a steel cable was fixed at 2/3 of the panel height at the center of the transverse section on one end and attached to a restraint frame on the other end. The cable was equipped with a load cell to measure the applied force along the cable. The displacement was measured at the location where the cable was fixed. The test was carried out in three phases. In Phase 1, the cable was pulled horizontally in order to form a cracked surface at the bottom of the specimen. In Phase 2, the cable was released to obtain a standing panel as in the initial configuration. Finally, in Phase 3, the cable was pulled horizontally and statically in displacement controlled conditions.

The LDPM parameters used in this study were calibrated in [60] on diagonal compression performed on a similar stone masonry mix composition. All the model parameters and the parameters related to the geometrical characterization can be found in details [60] and in [61], and are therefore not reported here for the sake of brevity. Fig. 2 shows the random stone-particle placement inside the three panels. One can note that the base of the specimen and the panel were modeled using one LDPM mesh. At the bottom of the base, the particles were fixed in translations and rotations. A velocity was applied directly to a set of particles at 2/3 of the

Panel number	Width B [mm]	Height H [mm]	Thickness D [mm]	Slenderness λ [-]
P1	900	900	300	3
P2	900	1100	220	5
P3	900	1500	300	5

Table 1: Dimensions of the panels for model validation.

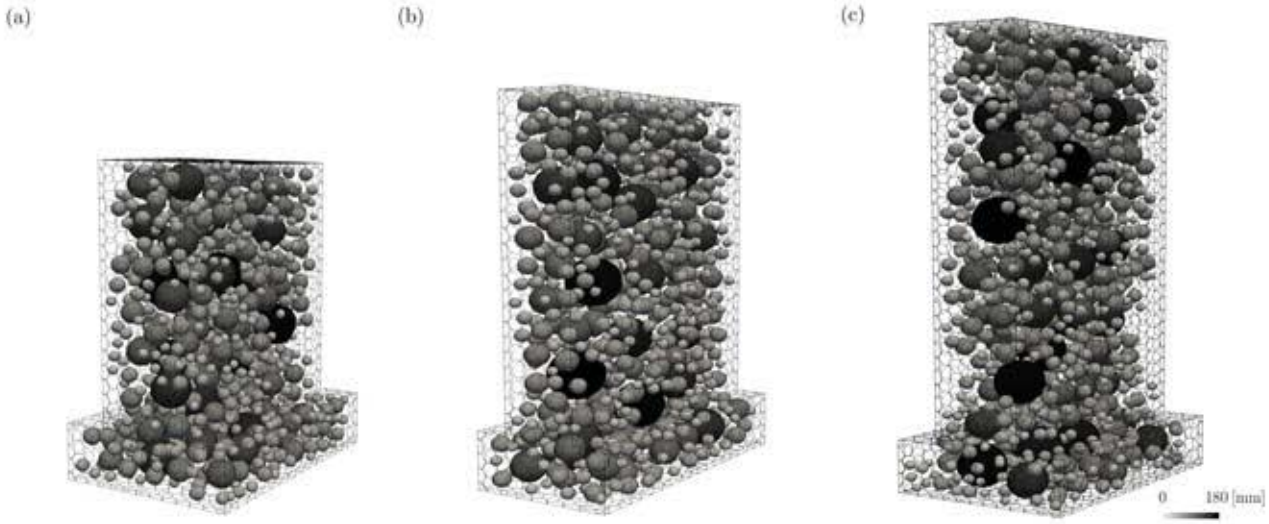

Figure 2: Spatial distribution of stone-particles in the three panels: (a) panel 1, (b) panel 2, (c) panel 3.

panel height to reproduce the experimental setup. Its magnitude was chosen low enough to obtain a quasi-static simulation. Two sets of simulations were performed. The first strategy was to reproduce the same testing procedure as in the experiments, i.e. in three phases. The second strategy, less computationally expensive, was to apply the static load directly to the uncracked specimen, from the beginning of the test, up to cracking and overturning of the panel. Finally, for all the simulations, three different stone distributions within the volume of the panels were used to capture the experimental scatter due to the spatial variability of stone size and distribution. Thus, the results shown afterwards are the average of the three individual results.

2.2.2 Numerical results and discussion

Fig. 3 refers to panel 2 and it shows the results of the two modeling strategies previously stated. One can see that replicating the experimental procedure (see Fig. 3a) and loading directly the sample from the initial uncracked configuration (see Fig. 3b) provide identical results. Fig. 3b shows clearly the fracturing part of the test followed by the overturning or rocking phenomenon once the fracture is formed. In order to save computational time, the second strategy was used to generate the results presented next.

Fig. 4 shows the load-displacement curves of for the three panels. One can see that the numerical results well predict the experimental data, especially for panels 1 and 2. In terms of fracture, all the three specimens failed at the base (see Fig. 5) as expected and observed in the experimental tests of panels 1 and 2. For panel 3, experimentally, the fracture formed at a height of 300 mm from the base, where the stones were not well interlocked. This unexpected failure

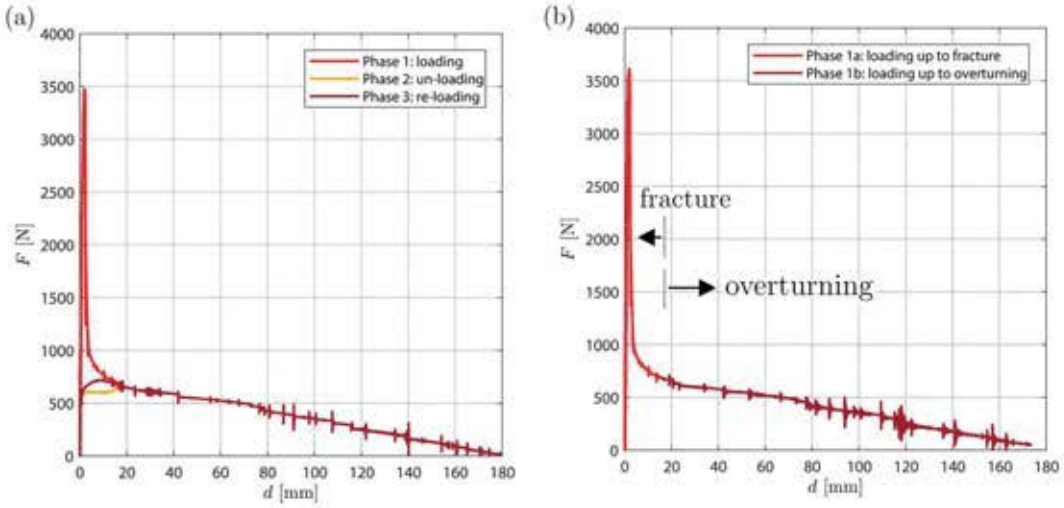

Figure 3: Force versus displacement curves for Panel 2: (a) Three phases loading; (b) Loading directly from the initial uncracked configuration

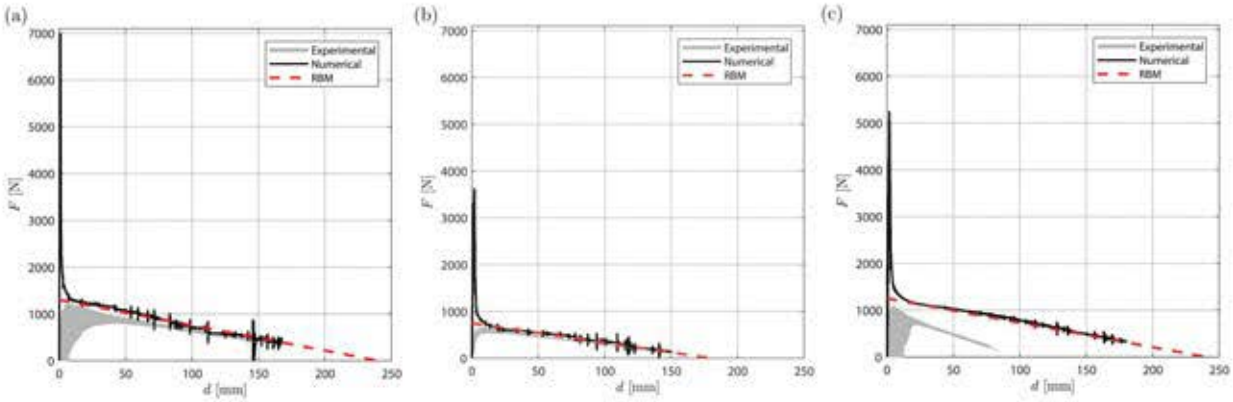

Figure 4: Force versus displacement curves in: (a) panel 1; (b) panel 2; (c) panel 3.

could be due to the preparation of the panels. The numerical response for panel 3 therefore overestimates the experimental results as the predicted failure occurred at the base.

For all the panels, the load-displacement trend is identical. First, the load increases linearly which represents the initial elastic phase. Next, a non-linear phase is reached while the load keeps increases which relates to the crack formation. In the post-peak regime, a softening behavior is observed and corresponds to the fracture propagation. Finally, a decreasing linear trend is observed for the load as the displacement increases. This phase characterizes the overturning process. One can analyze the latter phase using non-linear kinematic analysis, and more specifically the rigid-block displacement-based method.

Fig. 4 shows the results from the analytical method obtained from the kinematic analysis. The parameters used to perform the linear and non linear kinematic analyses are reported in Table 2. One can see that there is an excellent agreement with the numerical results. It is interesting to note that the horizontal force associated with the activation of the overturning F_0 are close to the kink point predicted by LDPM.

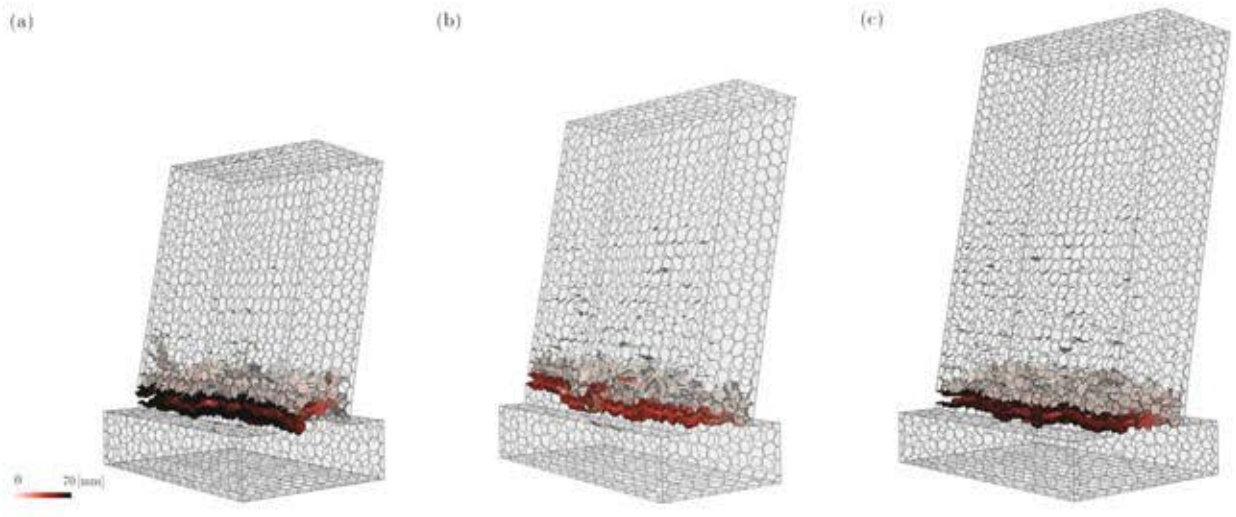

Figure 5: Total crack opening in: (a) panel 1; (b) panel 2; (c) panel 3.

Table 2: Parameters used to perform the linear and non linear kinematic analyses: initial horizontal multiplier α_0, ultimate displacement d_u, participant mass fraction e^*, initial spectral acceleration a_0^*, initial horizontal force F_0. The initial condition is referred to the activation of the overturning and the ultimate condition is associated with the loss of the overall equilibrium.

Panel Number	α_0 [-]	d_u [mm]	e^* [-]	a_0^* [m/s^2]	F_0 [N]
P1	0.333	240	1.0	1.962	1252
P2	0.200	180	1.0	1.962	673
P3	0.200	240	1.0	3.270	1252

3 APPLICATION TO COMPLEX STRUCTURES

3.1 Local bending mechanism

3.1.1 Vertical bending mechanism

Design codes usually require the analysis of local collapse mechanism in unreinforced masonry walls for the assessment of seismic vulnerability [70]. Vertical bending mechanism was here considered as a first application of the numerical model and can be viewed as an alternative to kinematic analysis. The vertical bending mechanism is characterized by the fracture and the out-of-plane simultaneous rotation of two blocks of a facade with respect to the horizontal axis (often located at mid-height of the panel). This bending mechanism is observed for single or multi-story walls and the mechanical response depends on the effectiveness of the connection system with floors and the presence of openings or discontinuities.

For the simulation of vertical bending, two wall geometries were considered to be representative of real masonry walls. The first wall geometry was a one-story wall. It had a height of 3,000 mm, a thickness of 500 mm and a width 4,000 mm. Using this geometry, two cases were considered: case 1B-NO without openings and case 1B-O with openings. The dimensions of the openings were chosen to replicate the presence of windows (of 1,200 mm height, 500 mm thickness, 800 mm width) and doors (of 2,400 mm height, 50 mm thickness and 800 mm width). The second wall geometry was a two-story wall. It had a height of 6,000 mm, a thickness of 500 mm and a width 4,000 mm. Again, two cases were considered: case 2B-NO without openings and case 2B-O with openings. For all the walls, the translation and rotation of the stone-particles

were fixed on the bottom and the top sides. The load was applied in quasi-static conditions as a velocity prescribed to the surface particles at mid-height of the walls. Finally in order to consider self-weight, gravity load was applied prior to testing.

3.1.2 Results and discussion

Fig. 6 and Fig. 7 show the results of the simulations, for one-story and two-story walls, respectively.

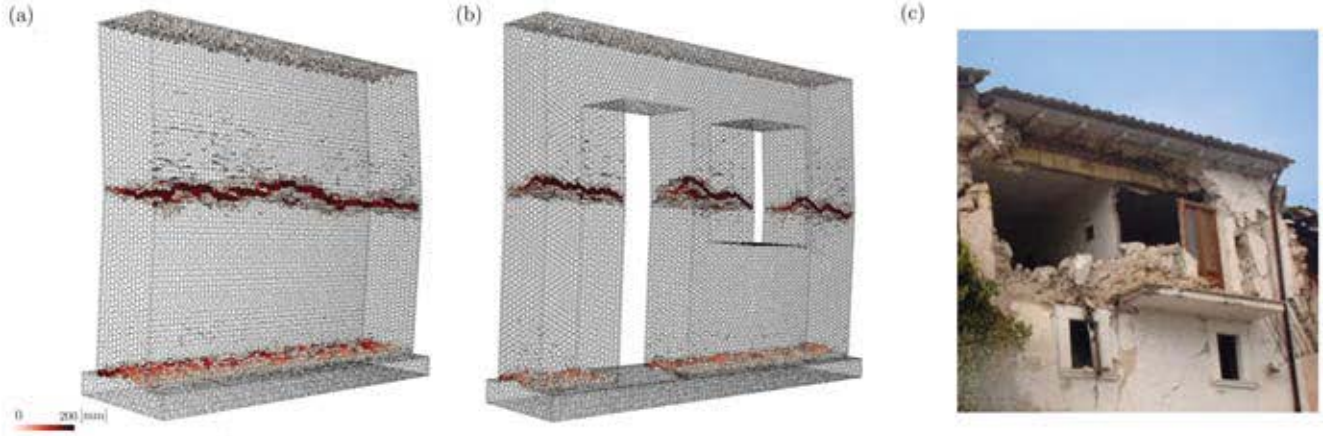

Figure 6: Total crack opening: (a) one-story wall with no openings (1B-NO); (b) one-story wall with openings (1B-O); (c) Example of one-story bending mechanisms caused by the 2009 L'Aquila earthquake (Arch. Fot. Vice Comm. Del. Beni Culturali - Sisma Abruzzo 2009).

One can see that the main failure occurs at mid-height for the no-opening cases, with a secondary damage along the base (see Fig. 6a and Fig. 7a). In the cases with openings, one can notice that the crack occurs at about mid-height for the one-story wall (see Fig. 6b). For the two-story panel, the presence of windows affects the position of the main fracture, which is located close to the bottom of the windows and follows the discontinuity due to their inclusion (see Fig. 7b). Fig. 7d shows the load-displacement curves for the four cases. The trend is the same for all the walls. The load increases in an elastic phase and reaches a peak value. Next, a softening behavior is observed. As expected, the peak loads for the smaller walls are higher than the two-story panels. A reduction of the stiffness and the bearing capacity is observed when openings are considered. In particular, for the one-story bending mechanism, the stiffness and the bearing capacity decrease by 3.5% and 37.1%, respectively. For the two-story bending mechanism, the stiffness and the bearing capacity decrease of 6.9% and 16.4%, respectively.

3.2 Combined and Complex Mechanisms

3.2.1 Numerical modeling

In the analysis of local collapse mechanisms, all the possible failure mechanisms need first to be identified before being analyzed, for example using kinematic analysis. In more complex cases, such a process is impossible and simplified analytical methods are no longer satisfactory for an accurate study. In real structures, masonry walls are always in interaction with other structural elements. For example, the walls might be located withing the continuity of a facade. There might also be transversal walls, floors and roofs attached to the main panel subjected

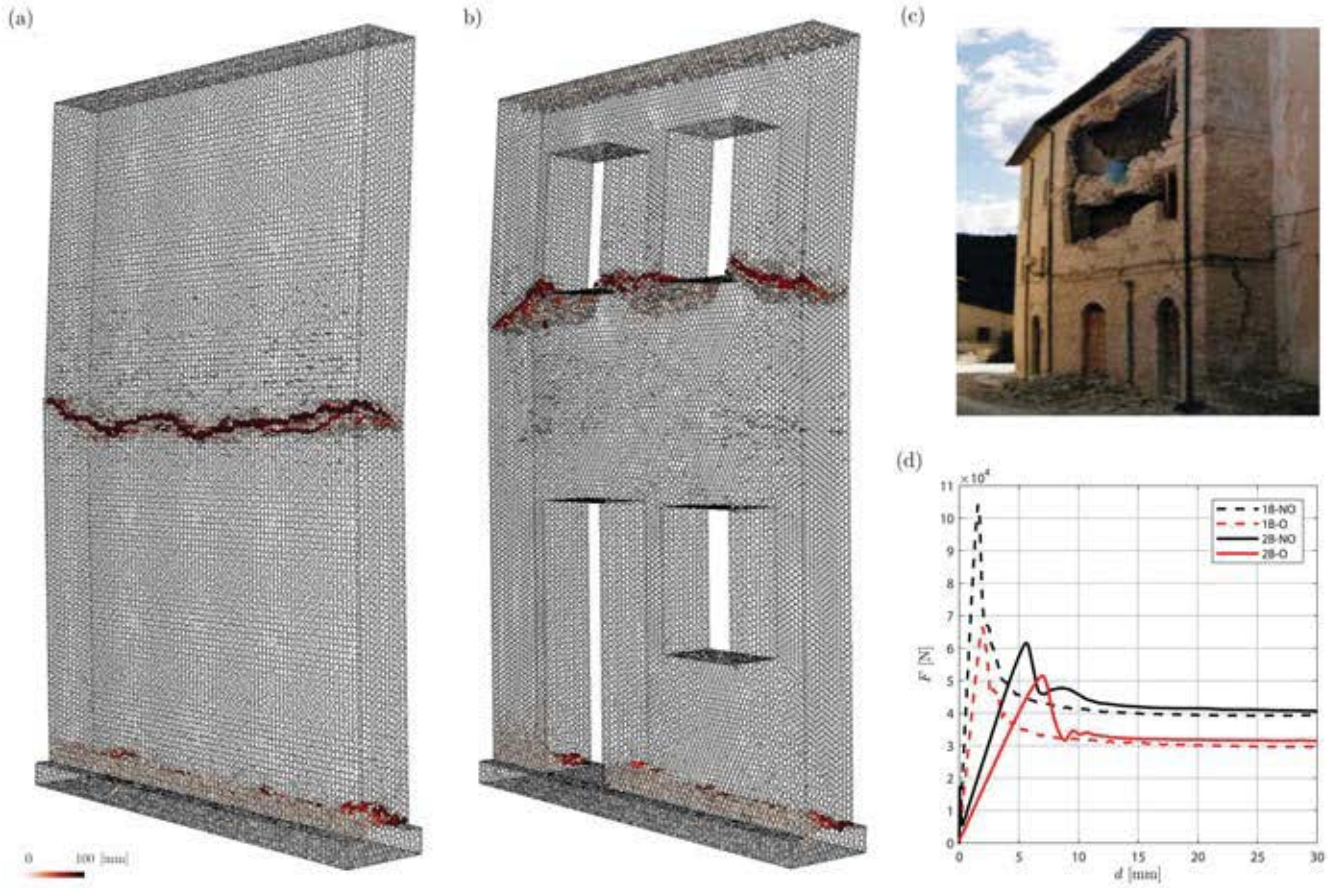

Figure 7: Total crack opening: (a) two-story wall with no openings (2B-NO); (b) two-story wall with openings (2B-O); (c) Example of two-story bending mechanisms caused by the 2009 L'Aquila earthquake (Arch. Fot. Vice Comm. Del. Beni Culturali - Sisma Abruzzo 2009); (d) force versus displacement curves for Cases 1B-NO, 1B-O, 2B-NO and 2B-O.

to out-of-plane loading. Moreover, masonry walls are usually the result of different stratification phases occurred over the course of many centuries. Here, three modeling strategies were adopted to reproduce different structural and time relations between the panels: (i) relation of contemporaneity (STRC), (ii) relation of anteriority (STRA) and (iii) relation of posteriority (STRP). In total, seven different cases were considered and they were based on the two-story bending wall with openings presented earlier.

STRC panels were modeled to replicate walls belonging to the same historical period. A single LDPM mesh was used and three sets of boundary conditions were considered to model different degrees of toothing between the walls. Fig. 8a, b, c show the models ordered by increasing level of constraint. The first model assumed the particles at the bottom surface to be fixed (see Fig. 8a). The second model assumed the particles at the bottom surface and the back surfaces of the transversal walls to be fixed (see Fig. 8b). The third model assumed the particles at the bottom surface, the back surfaces of the transversal walls and the lateral surfaces of the lateral walls to be fixed (see Fig. 8c).

STRP panels were modeled to replicate walls built after the adjacent structures. The main wall and the lateral-transversal walls were modeled using three separate LDPM meshes. All the particles at the bottom surface, the back surfaces of the transversal walls, and the lateral surfaces of the lateral walls were assumed to be fixed. A sliding with friction constraint model [59] was used at the interface between the panels. In order to simulate different levels of toothing

between the walls, two different friction conditions were adopted. High friction conditions were simulated using a static friction factor $s_{ff} = 0.13$ and a dynamic friction factor $d_{ff} = 0.015$ (see Fig. 8d), whereas low friction conditions were simulated with $s_{ff} = 0.03$ and a $d_{ff} = 0.0084$ (see Fig. 8e).

STRA panels were modeled to replicate walls built before the adjacent structures. The central-transversal walls and the lateral walls were modeled using three separate LDPM meshes. The structure composed by the main central panel and the transversal walls was assumed to belong to a previous historical period with respect to the lateral walls. The particles belonging to the bottom surface, to the back surfaces of the transversal walls and the lateral surfaces of the lateral walls were fixed. In order to simulate different levels of toothing between walls, the same sliding with friction algorithm was used and applied to the discontinuity surfaces between the panels. The same parameters for the friction mode were assumed, i.e. high friction (see Fig. 8f) and low friction (see Fig. 8g).

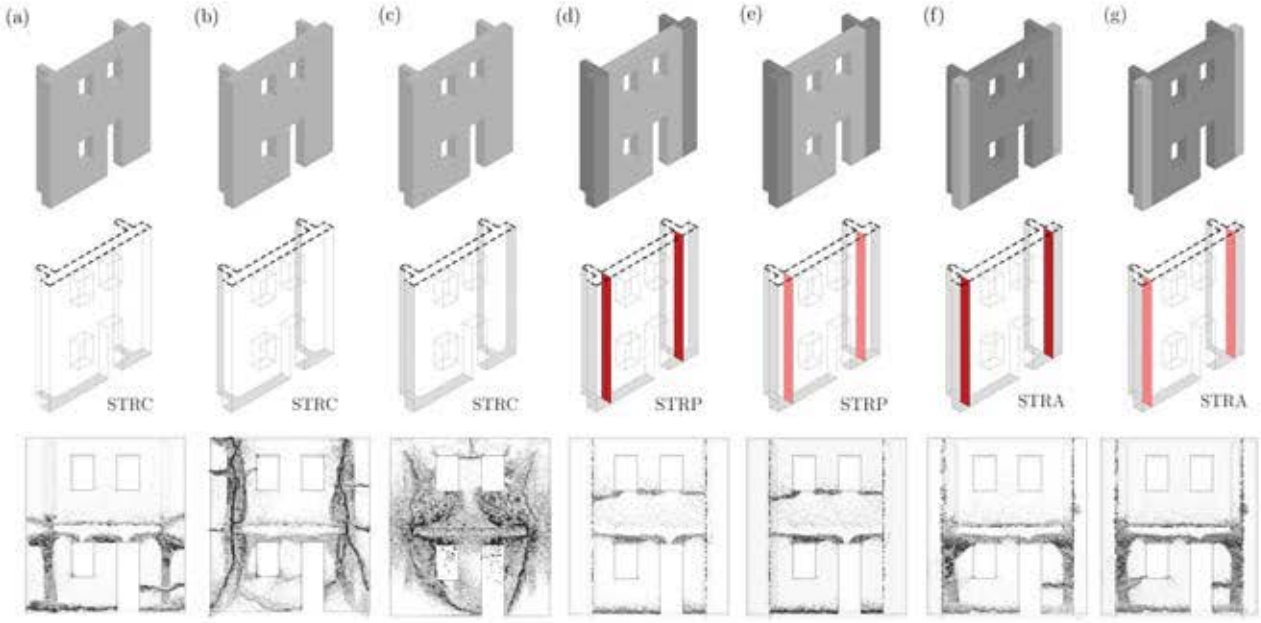

Figure 8: Geometry (top), boundary conditions (middle) and crack contours (bottom). In the middle row, the gray areas represent surfaces with all constrained displacements, the areas included within the black dotted lines represent the surfaces with horizontal displacements constrained in the out-of-plane direction and the red areas represent frictional interfaces (dark red for high friction and light red for low friction).

For all the simulated walls, the load was applied in quasi-static conditions by prescribing a velocity to particles of 300 mm height, between 2,700 mm and 3,000 mm, to reproduce the horizontal load of a floor activated by the seismic action. On top of the wall (at the second floor), the translations of the particles were constrained horizontally in the out-of-plane direction. The remaining boundary conditions and geometrical features of the structure are identical to the ones reported for the local bending mechanism case with opening case 2B-O.

3.2.2 Results and discussion

Fig. 8 and Fig. 9a, b, c, d, e, f show the damage distribution in the structures for the different configurations. Little similarities could be found with the local bending mechanism analyzed earlier. The fracture obviously depend on the boundary conditions and the connections between

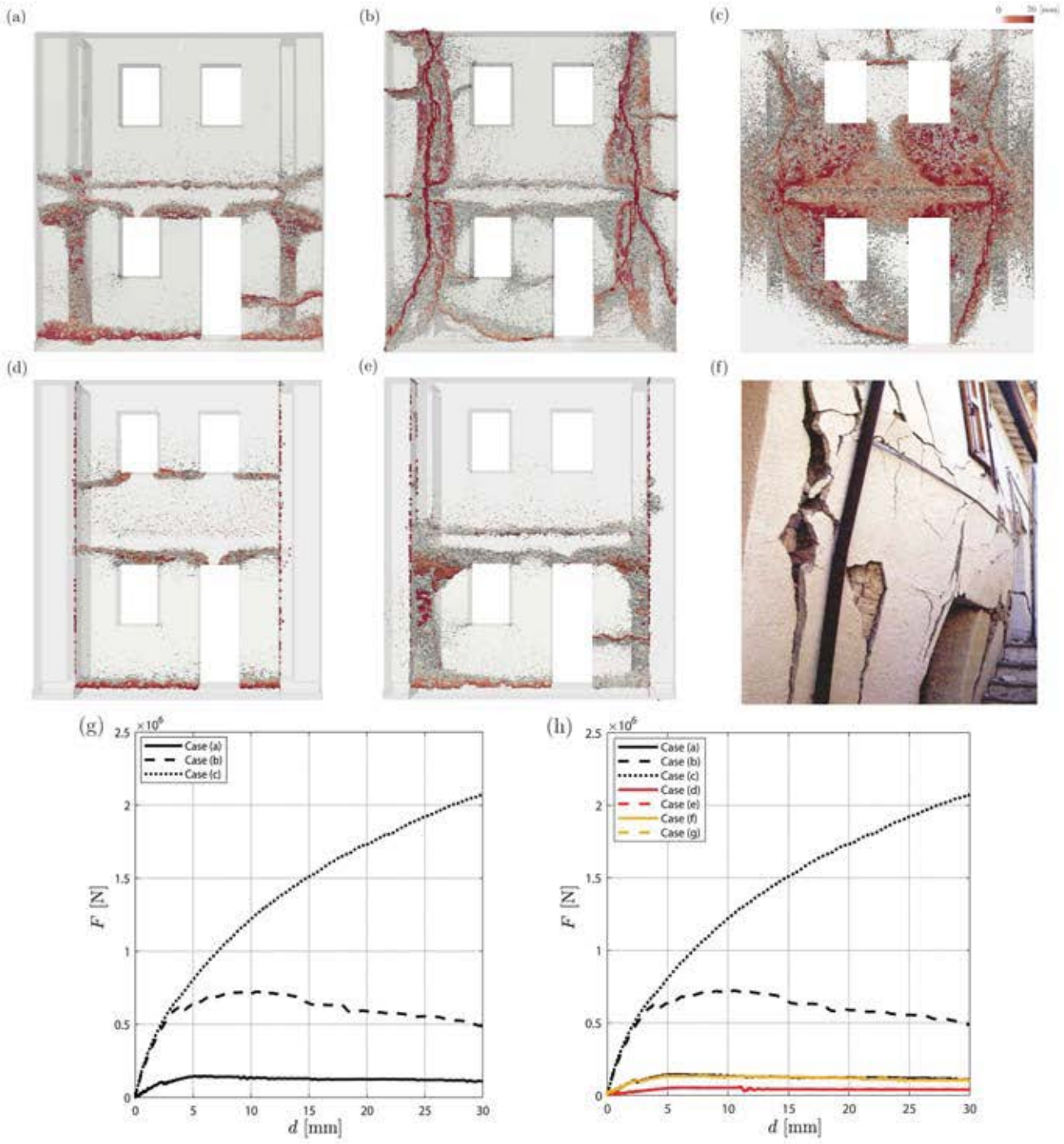

Figure 9: Total crack opening: (a), (b) and (c) STRC; (d) STRP; (e) STRA; (f) example of a complex mechanism (Arch. Fot. Vice Comm. Del. Beni Culturali - Sisma Abruzzo 2009). Force versus displacement curve: (g) for the cases (a), (b), (c); (h) for all the cases.

the central panel and the lateral and back walls. The damage in the case depicted in Fig. 8f, Fig. 8g and Fig. 9e is similar to the damage in the case shown in Fig. 8a and Fig. 9a. The reason might be that the continuity between the central and the transversal walls generates cracks in the lower floor as well as in the upper part. The main cracks in the cases depicted in Fig. 8b and Fig. 9b are vertical. On the contrary, the damage is distributed through the entire wall and are slightly concentrated in the central area (see Fig. 8c and Fig. 9c). In terms of quantitative analysis, Fig. 9g shows the load-displacement curves for the cases depicted in Fig. 8a, b, c. Fig. 9h shows all the curves. The more constrained case (see Fig. 8c and the least constrained one (see Fig. 8d define the upper and lower bound curves, respectively. One can deduce from these results that the choice of the correct boundary conditions in the analysis of such structures is complex and only a good estimation might be made. It also underlines the importance of performing accurate surveys to understand the architectural configuration and the historical evolution of the building.

4 CONCLUSIONS

The proposed Lattice Discrete Particle Model (LDPM) is presented, validated and used in the prediction of the mechanical behavior of unreinforced masonry structures in out-of-plane loading conditions. The model was first validated against experimental data and compared with nonlinear kinematic analysis (rigid-block displacement-based method). LDPM was then used to analyze more complex structures. Local bending mechanism was studied on walls with and without openings. The interaction between adjacent walls were also taken into account. The proposed numerical model is able to predict realistic fracture pattern in complex structures. On the basis of the results discussed in this paper, the following conclusions can be drawn.

- The damage distribution resulting from the collapse of masonry walls is well captured by LDPM.
- LDPM results were verified experimentally and with kinematic analysis. This suggests the use of this model to perform limit analysis for the assessment of local collapse mechanisms.
- Unlike typical kinematic analysis, LDPM does not require to identify a priori local collapse mechanisms. More complex configurations impossible to investigate analytically can also be considered.
- The presence of openings within walls and the application of adequate boundary conditions greatly affect the stiffness and bearing capacities of the walls.
- The results of this paper underlines the necessity to perform accurate in-field surveys in order to correctly model real masonry walls under out-of-plane loading.

REFERENCES

[1] G. Magenes, G. M. Calvi, In-plane seismic response of brick masonry walls, Earthquake engineering & structural dynamics 26 (11) (1997) 1091–1112.

[2] A. Menon, G. Magenes, Out-of-plane seismic response of unreinforced masonry: definition of seismic input, Rose School, IUSS Press, 2008.

[3] T. M. Ferreira, A. A. Costa, A. Costa, Analysis of the out-of-plane seismic behavior of unreinforced masonry: A literature review, International Journal of Architectural Heritage 9 (8) (2015) 949–972.

[4] K. Lang, H. Bachmann, On the seismic vulnerability of existing unreinforced masonry buildings, Journal of Earthquake Engineering 7 (03) (2003) 407–426.

[5] P. Morandi, G. Magenes, Second order effects in out-of-plane strength of urm walls subjected to bending and compression, ROSE Report (2006).

[6] A. A. Costa, A. Arêde, A. Costa, C. S. Oliveira, In situ cyclic tests on existing stone masonry walls and strengthening solutions, Earthquake Engineering & Structural Dynamics 40 (4) (2011) 449–471.

[7] A. A. Costa, A. Arêde, A. Costa, C. S. Oliveira, Out-of-plane behaviour of existing stone masonry buildings: experimental evaluation, Bulletin of Earthquake Engineering 10 (1) (2012) 93–111.

[8] D. D'Ayala, E. Speranza, Definition of collapse mechanisms and seismic vulnerability of historic masonry buildings, Earthquake Spectra 19 (3) (2003) 479–509.

[9] M. R. Valluzzi, On the vulnerability of historical masonry structures: analysis and mitigation, Materials and structures 40 (7) (2007) 723–743.

[10] R. Gabellieri, P. Diotallevi, L. Landi, Effect of diaphragm flexibility on the dynamic behaviour of unreinforced masonry walls in out-of-plane bending, in: Proceedings of the 15th World Conference on Earthquake Engineering, 2012, pp. 24–28.

[11] M. Gallonelli, Dynamic response of masonry buildings with rigid or flexible floors, Ph.D. thesis, Master Thesis, Rose School (2007).

[12] S. K. Jain, P. C. Jennings, Analytical models for low-rise buildings with flexible floor diaphragms, Earthquake engineering & structural dynamics 13 (2) (1985) 225–241.

[13] O. Penner, K. J. Elwood, Out-of-plane dynamic stability of unreinforced masonry walls in one-way bending: shake table testing, Earthquake Spectra 32 (3) (2016) 1675–1697.

[14] D. F. Peralta, J. M. Bracci, M. B. D. Hueste, Seismic behavior of wood diaphragms in pre-1950s unreinforced masonry buildings, Journal of Structural Engineering 130 (12) (2004) 2040–2050.

[15] C. C. Simsir, Influence of diaphragm flexibility on the out-of-plane dynamic response of unreinforced masonry walls, University of Illinois at Urbana-Champaign, 2004.

[16] A. Tena-Colunga, D. P. Abrams, Seismic behavior of structures with flexible diaphragms, Journal of Structural Engineering 122 (4) (1996) 439–445.

[17] S. Casolo, G. Uva, Nonlinear analysis of out-of-plane masonry façades: full dynamic versus pushover methods by rigid body and spring model, Earthquake Engineering & Structural Dynamics 42 (4) (2013) 499–521.

[18] G. D. Felice, R. Giannini, Out-of-plane seismic resistance of masonry walls, Journal of earthquake engineering 5 (02) (2001) 253–271.

[19] G. de Felice, Out-of-plane seismic capacity of masonry depending on wall section morphology, International Journal of Architectural Heritage 5 (4-5) (2011) 466–482.

[20] A. Giuffrè, A mechanical model for statics and dynamics of historical masonry buildings, in: Protection of the architectural heritage against earthquakes, Springer, 1996, pp. 71–152.

[21] P. B. Lourenço, J. G. Rots, Multisurface interface model for analysis of masonry structures, Journal of engineering mechanics 123 (7) (1997) 660–668.

[22] V. Giamundo, V. Sarhosis, G. Lignola, Y. Sheng, G. Manfredi, Evaluation of different computational modelling strategies for the analysis of low strength masonry structures, Engineering Structures 73 (2014) 160–169.

[23] J. Heyman, The stone skeleton, International Journal of solids and structures 2 (2) (1966) 249–279.

[24] J. Heyman, The Mansonry Arch, 1982.

[25] A. Giuffrè, Letture sulla meccanica delle murature storiche. (1991).

[26] L. Restrepo-Vélez, A simplified mechanics-based procedure for the seismic risk assessment of unreinforced masonry buildings, Individual Study (2003).

[27] C. Casapulla, Resistenze attritive in una parete muraria soggetta ad azioni normali al suo piano medio, in: L'Ingegneria Sismica in Italia; Proc. 9th nat. conf., Torino, 20-23 September 1999, 1999.

[28] L. Picchi, Risposta sismica per azioni fuori dal piano di pareti murarie, Graduation Thesis, University of Pavia (2002).

[29] G. A. Cundari, G. Milani, Homogenized and heterogeneous limit analysis model for pushover analysis of ancient masonry walls with irregular texture, International Journal of Architectural Heritage 7 (3) (2013) 303–338.

[30] S. Tiberti, G. Milani, 2d pixel homogenized limit analysis of non-periodic masonry walls, Computers & Structures 219 (2019) 16–57.

[31] S. Tiberti, G. Milani, 3d voxel homogenized limit analysis of single-leaf non-periodic masonry, Computers & Structures 229 (2020) 106186.

[32] S. Tiberti, G. Milani, 3d homogenized limit analysis of non-periodic multi-leaf masonry walls, Computers & Structures 234 (2020) 106253.

[33] K. T. Doherty, An investigation of the weak links in the seismic load path of unreinforced masonary buildings, Ph.D. thesis (2000).

[34] M. Tomaževič, Seismic resistance verification of masonry buildings: Following the new trends, 1997.

[35] G. W. Housner, The behavior of inverted pendulum structures during earthquakes, Bulletin of the seismological society of America 53 (2) (1963) 403–417.

[36] M. Priestley, R. Evison, A. Carr, Seismic response of structures free to rock on their foundations, Bulletin of the New Zealand National Society for Earthquake Engineering 11 (3) (1978) 141–150.

[37] D. Liberatore, G. Spera, Response of slender blocks subjected to seismic motion of the base: description of the experimental investigation, in: 5th International Symposium on Computer Methods in Structural Masonry, Rome, 2001, pp. 117–124.

[38] J. Zhang, N. Makris, Rocking response of free-standing blocks under cycloidal pulses, Journal of Engineering Mechanics 127 (5) (2001) 473–483.

[39] L. Sorrentino, S. Kunnath, G. Monti, G. Scalora, Seismically induced one-sided rocking response of unreinforced masonry façades, Engineering structures 30 (8) (2008) 2140–2153.

[40] O. A. Shawa, G. de Felice, A. Mauro, L. Sorrentino, Out-of-plane seismic behaviour of rocking masonry walls, Earthquake Engineering & Structural Dynamics 41 (5) (2012) 949–968.

[41] I. N. Psycharis, Dynamic behaviour of rocking two-block assemblies, Earthquake Engineering & Structural Dynamics 19 (4) (1990) 555–575.

[42] P. D. Spanos, P. C. Roussis, N. P. Politis, Dynamic analysis of stacked rigid blocks, Soil Dynamics and Earthquake Engineering 21 (7) (2001) 559–578.

[43] R. Gabellieri, L. Landi, P. Diotallevi, A 2-dof model for the dynamic analysis of unreinforced masonry walls in out-of-plane bending, in: Proc. of the 4th ECCOMAS Thematic Conference on Computational Methods in Structural Dynamics and Earthquake Engineering, 2013.

[44] H. Derakhshan, M. C. Griffith, J. M. Ingham, Out-of-plane behavior of one-way spanning unreinforced masonry walls, Journal of Engineering Mechanics 139 (4) (2011) 409–417.

[45] S. Lagomarsino, Seismic assessment of rocking masonry structures, Bulletin of earthquake engineering 13 (1) (2015) 97–128.

[46] S. Casolo, G. Milani, A simplified homogenization-discrete element model for the non-linear static analysis of masonry walls out-of-plane loaded, Engineering Structures 32 (8) (2010) 2352–2366.

[47] P. Lourenço, Computational strategy for masonry structures, Delft University of Technology and DIANA Research (1996).

[48] A. W. Page, Finite element model for masonry, Journal of the Structural Division 104 (8) (1978) 1267–1285.

[49] G. Milani, P. Lourenço, A. Tralli, Homogenization approach for the limit analysis of out-of-plane loaded masonry walls, Journal of structural engineering 132 (10) (2006) 1650–1663.

[50] P. B. Lourenço, Computations on historic masonry structures, Progress in Structural Engineering and Materials 4 (3) (2002) 301–319.

[51] J. Lemos, Discrete element modelling of the seismic behaviour of stone masonry arches, Computer methods in structural masonry 4 (1998) 220–227.

[52] G. Sincraian, J. Lemos, C. Oliveira, Assessment of the seismic behavior of stone masonry aqueduct using the discrete element method, in: Proc. 11th European Conf. on Earthquake Engineering, 1998.

[53] A. Drei, C. S. Oliveira, P. Lourenço, P. Roca, The seismic behaviour of the "aqueduto da amoreira" in elvas using distinct element modelling, in: Proceedings of the 3rd International Seminar on Historical Constructions, Guimarães Portugal November 7–9, 2001, 2001, pp. 7–9.

[54] C. Oliveira, J. V. Lemos, G. Sincraian, Modelling large displacements of structures damaged by earthquake motions, European Earthquake Engineering 16 (3) (2002) 56–71.

[55] A. Alexandris, E. Protopapa, I. Psycharis, Collapse mechanisms of masonry buildings derived by the distinct element method, in: Proceedings of the 13th world conference on earthquake engineering, Vol. 59, 2004, p. 60.

[56] H. Nguyen, M. Pathirage, M. Rezaei, M. Issa, G. Cusatis, Z. P. Bažant, New perspective of fracture mechanics inspired by gap test with crack-parallel compression, Proceedings of the National Academy of Sciences (2020).

[57] H. T. Nguyen, M. Pathirage, G. Cusatis, Z. P. Bažant, Gap test of crack-parallel stress effect on quasibrittle fracture and its consequences, Journal of Applied Mechanics 87 (7) (2020).

[58] G. Cusatis, D. Pelessone, A. Mencarelli, Lattice discrete particle model (ldpm) for failure behavior of concrete. i: Theory, Cement and Concrete Composites 33 (9) (2011) 881–890.

[59] G. Cusatis, A. Mencarelli, D. Pelessone, J. Baylot, Lattice discrete particle model (ldpm) for failure behavior of concrete. ii: Calibration and validation, Cement and Concrete composites 33 (9) (2011) 891–905.

[60] M. Angiolilli, A. Gregori, M. Pathirage, G. Cusatis, Fiber Reinforced Cementitious Matrix (FRCM) for strengthening historical stone masonry structures: Experiments and computations, Engineering Structures 224 (2020): 111102.

[61] M. Mercuri, M. Pathirage, A. Gregori, G. Cusatis, Computational modeling of the out-of-plane behavior of unreinforced irregular masonry, Engineering Structures Engineering Structures 223 (2020): 111181.

[62] C. Ceccato, M. Salviato, C. Pellegrino, G. Cusatis, Simulation of concrete failure and fiber reinforced polymer fracture in confined columns with different cross sectional shape, International Journal of Solids and Structures 108 (2017) 216–229.

[63] M. Pathirage, F. Bousikhane, M. D'Ambrosia, M. Alnaggar, G. Cusatis, Effect of alkali silica reaction on the mechanical properties of aging mortar bars: Experiments and numerical modeling, International Journal of Damage Mechanics 28 (2) (2019) 291–322.

[64] L. Han, M. Pathirage, A-T. Akono, G. Cusatis, Lattice Discrete Particle Modeling of Size Effect in Slab Scratch Tests, Journal of Applied Mechanics 88, no. 2 (2021).

[65] E. A. Schauffert, G. Cusatis, Lattice discrete particle model for fiber-reinforced concrete. i: Theory, Journal of Engineering Mechanics 138 (7) (2011) 826–833.

[66] J. Smith, G. Cusatis, D. Pelessone, E. Landis, J. O'Daniel, J. Baylot, Discrete modeling of ultra-high-performance concrete with application to projectile penetration, International Journal of Impact Engineering 65 (2014) 13–32.

[67] M. Alnaggar, G. Cusatis, G. Di Luzio, Lattice discrete particle modeling (ldpm) of alkali silica reaction (asr) deterioration of concrete structures, Cement and Concrete Composites 41 (2013) 45–59.

[68] M. Pathirage, D. Bentz, G. Di Luzio, E. Masoero, G. Cusatis, The onix model: a parameter-free multiscale framework for the prediction of self-desiccation in concrete, Cement and Concrete Composites 103 (2019) 36–48.

[69] S. Degli Abbati, M. Rossi, S. Lagomarsino, Out-of-plane experimental tests on masonry panels, in: Proceedings of the 2nd European Conference on Earthquake Engineering and Seismology, 2014, pp. 25–29.

[70] Decreto del ministro delle infrastrutture 17 gennaio 2018. aggiornamento delle "norme tecniche per le costruzioni", Gazzetta Ufficiale della Repubblica Italiana.